Silicon Resistivity Impact on Surface Waves for Antenna on-Chip Applications

L. Delait[1], Z. Tian[2], M. Rack[1], S. Ma[1], Q. Courte[1], A. Rennings[2], C. Craeye[1], J.-P. Raskin[1], and D. Lederer[1]
[1]ICTEAM, Université catholique de Louvain, 1348 Louvain-la-Neuve, Belgium
[2]General and Theoretical Electrical Engineering (ATE), University of Duisburg-Essen,
CENIDE – Center for Nanointegration Duisburg-Essen, 47048 Duisburg, Germany

***Abstract*—In this paper, the impact of the substrate resistivity on surface waves (SW) is studied for antenna on-chip applications on metal-backed thick substrates. Three silicon (Si) substrates are studied: standard bulk (Std), high-resistivity (HR) and trap-rich (TR) HR. First, a substrate parameter extraction is conducted based on CPW lines and matched with simulations to obtain an electromagnetic model of the material stack. From this, the effect of the parasitic surface conduction (PSC) on the SW attenuation and the high efficiency achieved by the SW propagating through TR are demonstrated by analytically extracting the SW attenuation constant for each substrate. Finally, a dipole-slot antenna is analyzed. It is characterized for several die dimensions. This demonstrates the impact of the resistivity on the excited SW through the radiation pattern (RP) and the S_{11} variation with die dimension due to SW diffraction and reflection at the die edges. Among the studied Si-based substrates, antennas on TR demonstrate the highest RP and return loss dependency on the chip dimension, due to the low attenuation of the excited SW. This study highlights the promising use of TR substrates as a solution to support high-efficiency mm-wave on-chip antennas, under the condition that the excited SW are properly dealt with during the antenna/chip co-design process.**

Keywords*— Surface waves, substrate resistivity, trap-rich Si-based substrate, parasitic surface conduction (PSC), dipole-slot antenna, on-chip antenna, CPW line, grounded slab.

I. Introduction

On-chip Si antennas enable direct integration with front-end circuitry, reducing connection loss and parasitic effects while facilitating co-design. Yet, they often suffer from poor radiation efficiency and low gain due to the high permittivity and loss of commonly used silicon (Si) substrates. A widely used strategy is to shield the Si with a metal layer between the antenna and the substrate but this leads to reduced bandwidth and efficiency due to the proximity of such a reflector [1]. A solution is to place the metal plane below the substrate, making the antenna sensitive to the Si. In this case, the use of a low-loss Si is needed to avoid a drop of antenna efficiency [2]. Moving from standard (Std) to high-resistivity (HR) substrate helps to mitigate this effect. The improvement is however hindered by the parasitic surface conduction (PSC) effect, a thin highly conductive layer of free electrons attracted by the positive fixed oxide charges at the Si/SiO_2 interface [3], resulting in a degradation of the coplanar effective resistivity [4]. Trap-rich (TR) is a well-known solution which renders the interface resistive by introducing a layer of undoped polysilicon full of traps underneath the oxide [3]. On the other hand, if the metal-backed Si substrate is electrically thick (i.e. thickness $H_{Si} > 0.1\ \lambda_{Si}$, with λ_{Si} the TEM mode wavelength in Si) due to process or design constraints, significant surface waves (SWs) can be excited by the antenna within the metal/Si substrate/air stack. Those SWs may diffract from the chip edges, if uncontrolled, and distort the radiation pattern (RP) of the antenna [5], [6]. The impact of the resistivity and PSC on antenna performance has been studied in previous papers, highlighting an increased efficiency on thin substrates [2], [7]. However, the effect of the resistivity and PSC on the generated SW, which may play a predominant role in the radiation mechanism –particularly as the operating frequency is increased– has never been studied and is the scope of this paper. In this paper, three silicon substrates are studied: Std, HR and TR. First, a substrate parameter extraction is conducted in Section II based on CPW lines and matched with simulations to obtain an electromagnetic (EM) model of the non-homogenous material stacks used in this paper. The CPW characterization is particularly useful to model the PSC, whose parameters can vary depending on the process. Based on this model, Section III explains the effect of the resistivity and in particular of the PSC layer on SW propagation by extracting the SW attenuation constant for each substrate. Finally, in Section IV, the effects of the SWs are studied on a dipole-slot antenna that is used as a demonstrator. The excited SW is first analyzed through simulations. The dipole-slot is then characterized on dies of different dimensions to highlight the impact of the resistivity on the excited SW through the RP and reflection coefficient S_{11} variations with those dimensions. It is shown that the change in antenna RP and S_{11} responses are due to SW diffraction and reflection at the die edges, which are dependent on the die size.

II. Substrate Characterization Through CPWs

The considered substrates were characterized using CPWs fabricated alongside the dipole-slot antennas. S-parameter measurements were performed using an Agilent N5242A PNA-X vector network analyzer in the 10 MHz – 110 GHz frequency range to extract substrate parameters. A pair of GSG 67 GHz infinity probes from FormFactor along with an MPI probe station were used. The reference planes at the probe tips are determined through an LRRM calibration. The method developed in [8] is used to extract the equivalent RLGC parameters of the CPW from the measurements of several line lengths. Fig. 1 presents the extracted effective resistivity (ρ_{eff}) of the substrate, defined in [4], and RF losses (α) of the CPW lines measured on 4 identical dies for the three considered substrates.

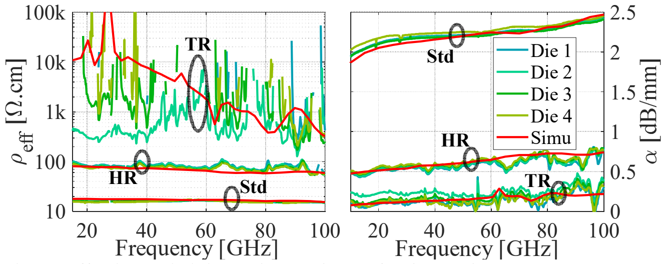

Fig. 1: Effective resistivity and CPW losses for the 3 substrates.

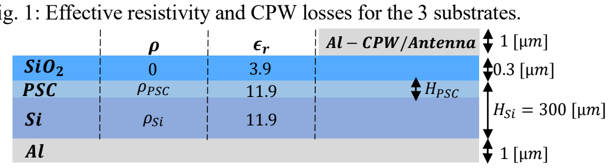

Substrate	ρ_{Si} [Ωcm]	ρ_{PSC} [Ωcm]	H_{PSC} [μm]
TR	5k	/	0
HR	5k	1	0.5
Std	12	/	0

Fig. 2: Material stack model for the 3 substrates.

2024 Asia-Pacific Microwave Conference (APMC) | 979-8-3503-6354-8/24/$31.00 ©2024 IEEE | DOI: 10.1109/APMC60911.2024.10867596

These are matched with simulations. The EM stacks used for the simulation are shown in Fig. 2. Good correlation between simulations and measurements is achieved. The HR substrate suffers from larger losses due to the presence of the PSC while the TR shows an effective resistivity close to its nominal one, leading to significantly reduced line losses α. From the obtained EM stack model, the impact of the PSC and resistivity on the SW can be analytically obtained.

III. Surface Wave Fundamental Mode Analysis

This section proposes an analytical extraction of the complex propagation constant of the fundamental SW mode TM_0 and validates the result with an EM simulation for each substrate. For higher order modes the extraction follows the same logic.

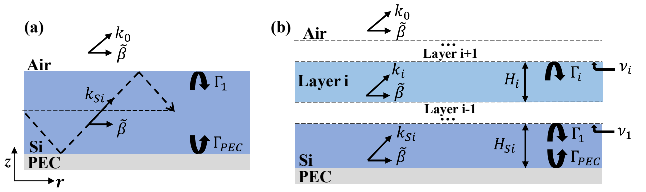

Fig. 3: Material stacks considered for the propagation constant extraction.

The propagation constant of the SW is obtained from the transverse resonance equation: After one period, the fields must be in phase [9]. As shown in Fig. 3(a), accounting for the transverse wave travelled distance as well as the 2 reflections Γ_1 and Γ_{PEC}, this translates mathematically into:

$$A\, e^{2j\pi N} = e^{-2j\sqrt{k_{Si}^2-\tilde{\beta}^2}\,H_{Si}} \cdot \Gamma_1 \cdot \Gamma_{PEC} \qquad (1)$$

With k_0 the free space wavenumber and for each material i, $k_i = \sqrt{\tilde{\varepsilon}_{r,i}}\,k_0$, $\tilde{\varepsilon}_{r,i} = \varepsilon_{r,i} - j\frac{1}{2\pi f \rho_i \varepsilon_0}$ and ρ_i its resistivity. $A \in \mathbb{R}$ accounts for the transverse wave attenuation and $N \in \mathbb{Z}$. This transcendental equation must be solved for the SW propagation constant $\tilde{\beta} = \beta - j\alpha$. In the case of the Si slab defined in Fig. 3(a), Γ_1 is given for the TM case by [9], [10]:

$$\Gamma_1 = \frac{\tilde{\varepsilon}_{r,Si}\sqrt{k_0^2-\tilde{\beta}^2} - \sqrt{k_{Si}^2-\tilde{\beta}^2}}{\tilde{\varepsilon}_{r,Si}\sqrt{k_0^2-\tilde{\beta}^2} + \sqrt{k_{Si}^2-\tilde{\beta}^2}} \qquad (2)$$

Considering a stack with layers atop the Si (shown in Fig. 3(b)), the expression of Γ_1 is modified in the TM case [10] as:

$$\Gamma_i = \frac{\nu_i + \Gamma_{i+1}\, e^{-2j\sqrt{k_{i+1}^2-\tilde{\beta}^2}\,H_{i+1}}}{1 + \Gamma_i\Gamma_{i+1}\, e^{-2j\sqrt{k_{i+1}^2-\tilde{\beta}^2}\,H_{i+1}}}, \text{ with } \nu_i = \frac{\tilde{\varepsilon}_{r,i}\sqrt{k_{i+i}^2-\tilde{\beta}^2} - \tilde{\varepsilon}_{r,i+1}\sqrt{k_i^2-\tilde{\beta}^2}}{\tilde{\varepsilon}_{r,i}\sqrt{k_{i+i}^2-\tilde{\beta}^2} + \tilde{\varepsilon}_{r,i+1}\sqrt{k_i^2-\tilde{\beta}^2}} \quad (3)$$

That should be solved iteratively by starting from the uppermost layer for which $\Gamma_i = \nu_i$. It should be noted that the square roots with negative imaginary parts should be selected in the previous equations to avoid field divergence as z goes to infinity.

For the 3 substrates defined in Fig. 2, the impact of the SiO_2 layer can be neglected as $\left|2\sqrt{k_{SiO_2}^2-\tilde{\beta}^2}\,H_{SiO_2}\right| \ll 1$. In the case of the substrates without PSC layer (i.e. Std and TR), this approximation allows the use of the expression of Γ_1 given by eq. (2) in eq. (1). In the case of the HR substrate, the presence of the PSC layer must be accounted for due to the non-negligible imaginary part of $\tilde{\varepsilon}_{PSC}$. In that case, eq. (3) should then be used in eq. (1), with the additional layer corresponding to the PSC, whose electrical parameters are listed in Fig. 2. Eq. (1) has been solved for the 3 substrates. The resulting attenuation constant for the fundamental SW mode is shown in Fig. 4(a) versus frequency (referred as Analytic solution). The analytical values are validated by simulating the stacks of Fig. 2 in HFSS, as shown in Fig. 4(b). The fundamental SW mode is excited using rectangular Wave-Ports separated by a distance L. PMC boundary conditions are imposed on the 2 lateral faces to confine power in the structure without altering the field distribution of the TM_0 mode and a radiation box is imposed on the top face. As the Wave-Ports are matched (i.e. $S_{11} < -45$ dB), the SW attenuation constant is obtained as: $\alpha = \frac{-1}{2L}\ln(|S_{21}|^2)$.

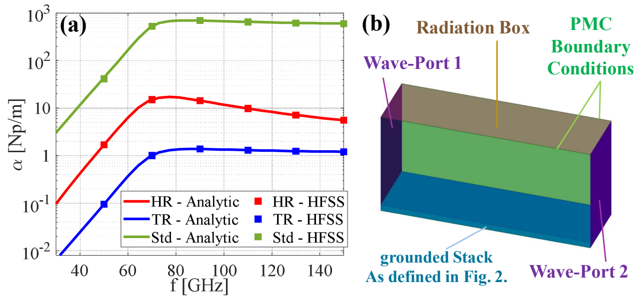

Fig.4: (a) Analytic and HFSS extracted attenuation constant of the TM_0 mode versus frequency for the 3 substrates defined in Fig. 2. (b) Simulation setup.

Fig. 4(a) compares the SW attenuation constant extracted from HFSS with the values obtained analytically from eq. (1). Excellent match is observed, validating the analytical model, and demonstrating the degradation of the SW due to PSC while travelling through the HR substrate. It can also be noted that, due to field confinement in the Si and the vanishing longitudinal fields as the frequency increases, the value of the attenuation constant tends towards that of the TEM mode in Si, i.e. $\alpha_{TEM} = -k_0\, \mathbb{I}\left\{\sqrt{\varepsilon_{r,Si} - j\frac{1}{2\pi f \rho_{Si}\varepsilon_0}}\right\}$. This is also true for HR as the fields at the Air-Si interface tend to zero as the frequency increases.

For each substrate, α reaches on this geometry a maximum around 76 GHz. This peak is more pronounced for the HR substrate for which the attenuation constant is more than 10 times higher than in the TR case at this frequency.

IV. Dipole-Slot Antenna On Thick Si

To experimentally illustrate the resistivity impact on the SW, a 75 GHz dipole-slot antenna has been designed as a demonstrator. This design was selected due to its simplicity of process and characterization with GSG probes. Besides, the operation frequency of 75 GHz allows avoiding the excitation of higher-order modes for this geometry.

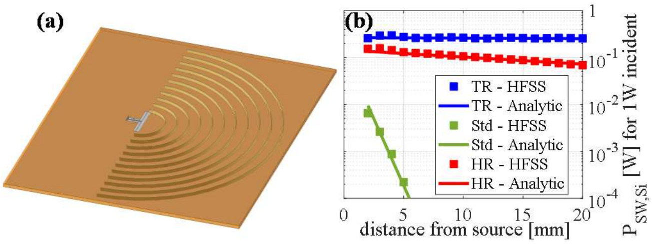

Fig.5: (a) Analyzed geometry. (b) SW power in Si at 75 GHz.

The antenna is first analyzed using HFSS. The SW power in the Si is computed by integrating the real part of the Poynting vector on the curved face of half-cylinders centered on the dipole slot (See Fig. 5(a)). A radiation boundary is imposed at the edges of the Si to avoid SW reflection. Fig. 5(b) compares for the 3 substrates the extracted power values at 75 GHz with the values obtained from the following expression: $P_{SW,Si}(R) = Ke^{-2\alpha R}$. In the latter, α is obtained from eq. (1) and K by fitting in the least-squares sense to the HFSS extracted power. A very high correlation between simulated and analytically extracted power is shown, demonstrating that the TM_0 mode excited by the antenna dominates the fields in the Si. Furthermore, the SW is propagating in TR with almost no attenuation, as expected. In comparison, 5 mm away from the source, the power is more than twice lower in the case of HR and divided by more than 100 for the Std. This is explained by the increased losses in the planar antenna itself as well as the higher attenuation of the excited SW, as described in Sections II and III, respectively.

The antenna was processed on four dies, each having an x-dimension of 13 mm and a variable y-dimension DieY of 10.5 mm + Δ = {0, 1 mm, 2 mm, 3 mm}. Dimensions are shown in Fig. 6(a). To highlight the RP and S_{11} dependency on the die dimension due to SW diffraction at the die edge, the four die size variants were fabricated on each type of substrate for a total of 12 test structures. A 5 mm-long CPW access has been used to mitigate the probe impact on the RP and has been de-embedded using the CPW characterization of Section II.

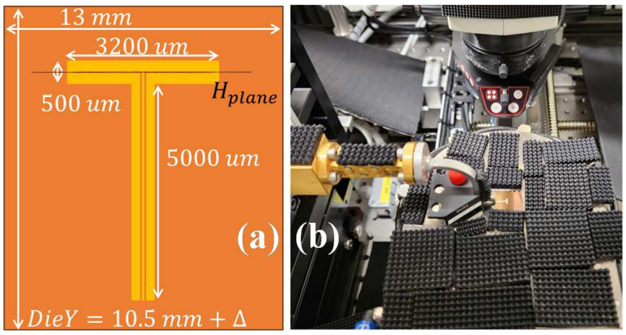

Fig. 6: (a) Processed Dipole-Slot. (b) On-wafer probe, absorbers and AUT.

For the far-field characterization, the spherical system presented in [11] was used. A close-up setup view is shown in Fig. 6(b). The gain of the antenna under test (AUT) was extracted by comparing the measured S_{21} parameter with a known horn antenna and compensating for the losses of the mm-wave probe using on-wafer calibration. To reduce the effect of the probe and metal chuck on the measured RP, they were covered with mm-wave absorber. The S_{11} and CPW access de-embedded RP at 75 GHz on the H-plane, defined in Fig. 6(a), are shown respectively in Figs. 7 and 8.

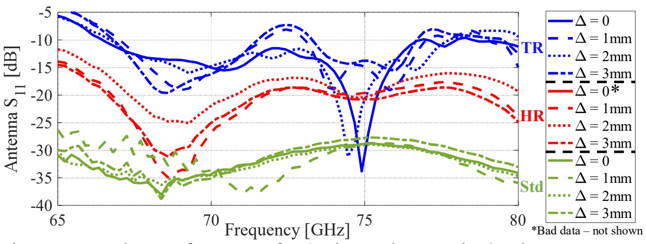

Fig. 7: Return loss vs frequency for 4 DieY values on the 3 substrates.

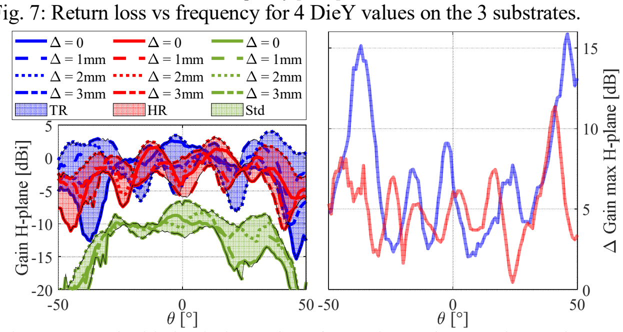

Fig. 8: De-embedded gain in H plane for 4 DieY values on the 3 substrates.

For the TR substrate, a strong dependency of S_{11} on the chip dimensions is observed. It is explained by the SW reflecting and diffracting at the chip edges, impacting the fields in the vicinity of the antenna, and in turn its input impedance. For the AUTs on the HR and Std substrates, very low dependency on S_{11} with DieY is observed. This is confirmed by the gain characterization for which the AUTs on TR exhibit higher peaks in gain variation compared with the ones on HR (Fig. 8), owing to the less attenuated SW diffracting at the chip edges. This corroborates the analysis of the SW power previously performed in Fig. 5. It must be noted that the gain for the AUTs on Std before CPW access de-embedding reaches values around -20 dBi. The observed gain variance in this case is explained by setup sensitivity and not SW diffraction at chip edge.

These results confirm the impact of the resistivity and PSC on the SW, as the SW power that reaches the chip edges is reduced for the cases of HR and Std compared to TR substrate, leading to lower RP and S_{11} parameter dependency on DieY.

V. Conclusion

In this article, the impact of the substrate resistivity on the SW, which plays a predominant role in the radiation mechanism of antennas on thick substrates, has been analyzed. Three Si substrates were studied: Std, HR and TR. First, a substrate parameter extraction was conducted based on CPW lines and matched with EM simulations. From this, a physical analysis of the SW attenuation has been performed for each substrate –including the development of an analytical model– demonstrating the effect of the PSC on the SW attenuation and the high efficiency achieved by the SW propagating through TR. Finally, a dipole-slot antenna has been characterized on several die dimensions to highlight the impact of the resistivity on the SW through RP and return loss dependency. Among the Si-based substrates, the TR substrate demonstrates an increased efficiency but also exhibits a stronger dependency of RP and return loss dependency on the chip dimension, due to the low attenuation of the excited SW. This demonstrates the promising use of TR substrates as a solution to support high-efficiency mm-wave on-chip antennas, under the condition that the excited SW are well considered during the antenna/chip co-design process.

References

[1] S. -Y. Tang et al., IEEE Trans. Antennas Propag., vol. 71, no. 9, pp. 7184-7195, Sept. 2023.
[2] N. André et al., IEEE Journ. Elec. Dev. Soc., vol. 7, pp. 393-397, 2019.
[3] M. Rack et al., IEEE Trans. Elec. Dev., vol. 68, no. 9, pp. 4598-4605, 2021.
[4] D. Lederer et al., Solid-State Elec., vol. 49, no. 3, pp. 491-496, 2005.
[5] F. Gianesello et al., Antenna-in-Package Technology and Applications, IEEE, pp. 179-218, 2020.
[6] N. G. Alexopoulos et al., IEEE Transactions on Microwave Theory and Techniques, vol. 31, no. 7, pp. 550-557, July 1983.
[7] E. Ojefors et al., IEEE Transactions on Microwave Theory and Techniques, vol. 55, no. 7, pp. 1467-1475, July 2007.
[8] G. Carchon et al., IEEE MTT-S Int. Microw. Symp. Dig., vol. 148, no. 5, pp. 285–290, 2001.
[9] H. Kogelnik, Integrated Optics, New York: Springer-Verlag, 1975.
[10] Orfanidis SJ., Electromagnetic waves and antennas, ch. 7, 2016.
[11] B. Sievert et al., IEEE Access, vol. 8, pp. 89680-89691, 2020.